Enhancement of electroluminescent properties of organic optoelectronic integrated device by doping phosphorescent dye*

Shu-ying Lei(雷疏影)[1,2], Jian Zhong(钟建)[1,2,†], Dian-li Zhou(周殿力)[1,2], Fang-yun Zhu(朱方云)[1,2], and Chao-xu Deng(邓朝旭)[1,2]

[1] State Key Laboratory of Electronic Thin Films and Integrated Devices, Chengdu 610054, China
[2] School of Optoelectronic Information, University of Electronic Science and Technology of China (UESTC), Chengdu 610054, China

(Received 4 June 2017; revised manuscript received 26 July 2017; published online 30 September 2017)

Organic optoelectronic integrated devices (OIDs) with ultraviolet (UV) photodetectivity and different color emitting were constructed by using a thermally activated delayed fluorescence (TADF) material 4, 5-bis(carbazol-9-yl)-1, 2-dicyanobenzene (2CzPN) as host. The OIDs doping with typical red phosphorescent dye [tris(1-phenylisoquinoline)iridium(III), $Ir(piq)_3$], orange phosphorescent dye {bis[2-(4-tertbutylphenyl)benzothiazolato-N, $C^{2'}$]iridium (acetylacetonate), $(tbt)_2Ir(acac)$}, and blue phosphorescent dye [bis(2, 4-di-fluorophenylpyridinato)-tetrakis(1-pyrazolyl)borate iridium(III), FIr6] were investigated and compared. The $(tbt)_2Ir(acac)$-doped orange device showed better performance than those of red and blue devices, which was ascribed to more effective energy transfer. Meanwhile, at a low dopant concentration of 3 wt.%, the $(tbt)_2Ir(acac)$-doped OIDs showed the maximum luminance, current efficiency, power efficiency of 70786 cd/m^2, 39.55 cd/A, and 23.92 lm/W, respectively, and a decent detectivity of 1.07×10^{11} Jones at a bias of -2 V under the UV-350 nm illumination. This work may arouse widespread interest in constructing high efficiency and luminance OIDs based on doping phosphorescent dye.

Keywords: organic optoelectronic integrated device, thermally activated delayed fluorescence host, phosphorescent dye, high luminance

PACS: 70.60.Fi, 85.60.Jb, 85.60.Gz, 73.61.Ph **DOI:** 10.1088/1674-1056/26/11/117001

1. Introduction

The research of organic photoelectronic devices has made significant progress in recent years. Common organic photoelectronic devices include organic light-emitting diodes (OLEDs),[1,2] organic photovoltaic devices (OPVs),[3] organic photodetectors (OPDs),[4,5] and organic thin film transistors (OTFTs). Among them, OLEDs have been widely used in solid-state lighting and full-color flat-panel displays, which are considered as the most ideal and potential display technology in the 21st century.[6–8] Meanwhile, OPDs have drawn wide interests due to their potential application in fields of biological sensing, solar astronomy, smoke/fire monitoring, and missile plume detection.[9,10] Nowadays, organic optoelectronic integrated devices (OIDs) with OLED and ultraviolet OPD dual functions become an important part of organic optoelectronics, since the integration of the two functions is helpful to reduce the device size and simplify the fabrication process.[11–13]

OIDs have two working modes, as shown in Fig. 1. For the OLED mode, under a forward voltage bias, the charge carriers are separately injected from the cathode and anode into the active layer to form excitons, which then requires an efficient radiative recombination of the molecular excitons. In terms of OPD mode, inversely, molecular excitons are formed with optical absorption and dissociated into free charge carriers in the active layer, then collected by the electrodes under a reverse bias. Obviously, the operating principle of OLED is contrary to that of OPD and the contrary exciton movement mechanisms make it hard to reach both high luminance and detectivity in OIDs.[14,15] Recently, much effort has been put into finding a practicable way to improve the luminance and detectivity of OIDs for practical application integrated device with UV photodetectivity and electroluminescence (EL) properties. Ali *et al.* showed a multilayer integrated device which gave a photoresponse of 77 mA/W at 390 nm and a maximum current efficiency of 2.2 cd/A for a brightness of 2200 cd/m^2.[16] Zhou *et al.* reported an OID with a high detectivity of 4.5×10^{12} Jones and a brightness of 7100 cd/m^2 using a two triplet–triplet annihilation featured material doping system.[17] Although OIDs have exhibited greatly enhanced detection performance, the electroluminescent performance is still low compared to the common OLED.

Nowadays, the thermally activated delayed fluorescence (TADF) materials are not only widely adopted to fabricate highly efficient OLEDs, but also used as the active layer to realize high performance OIDs.[15,18–21] Wang *et al.* reported a TADF-based integrated device which gave a detectivity of 1.4×10^{12} Jones and a brightness of 26370 cd/m^2 by inserting an exciton adjusting layer (EAL).[15] In our previous works, the importance of EAL- to TADF-based OIDs was analyzed.

*Project supported by the National Natural Science Foundation of China (Grant No. 61675041) and the National Science Funds for Creative Research Groups of China (Grant No. 61421002).

†Corresponding author. E-mail: zhongjian@uestc.edu.cn

© 2017 Chinese Physical Society and IOP Publishing Ltd

Great improvements in UV-detectivity (from 10^9 Jones to 10^{12} Jones) and luminance (from 5000 cd/m^2 to 25000 cd/m^2) were achieved by changing the varieties and thickness of the EAL materials.[22] However, the research on the utilization of the TADF-featured material as the host of phosphorescent dye has not been carried out so far. As is known, the strong spin–orbit coupling of electronic states induced by the heavy metal-atom effect of phosphorescent dyes can realize radiative decay of both singlet and triplet excitons for phosphorescence, leading to the theoretical internal quantum efficiency (IQE) of 100%.[23–25] However, phosphorescent dyes suffer from serious concentration quenching effect, which is required to be doped as a guest into the host material.[26] It should be pointed out that the singlet-triplet splits (ΔE_{ST}) of a TADF material is usually under 100 meV, lower than the conventional host materials, it is a kind of suitable host material for high-efficiency and low roll-off phosphorescent OLEDs.[27,28] Furthermore, the conversion of triplet excitons on TADF materials to singlet excitons on phosphors can be realized via reverse inter-system crossing (RISC) followed by long-radius Förster resonance energy transfer (FRET), so the OLEDs using TADF materials as the host can achieve efficient host-guest energy transfer in a low doping concentration.[29] Although it is an effective strategy to overcome exciton quenching and improve the EL performance of OLED by utilizing the model of energy transfer between the host and dopant materials, there are few works that apply this method for realizing high performance OIDs. Thus, a study of doping system for the OIDs, correlating with the energy transfer between the host and the dopant, is imperative.

In this work, the effect of a novel TADF-featured host material of 2CzPN on the performance of several typical phosphorescent dyes (including tris(1-phenylisoquinoline)iridium(III) [Ir(piq)$_3$], bis[2-(4-tertbutylphenyl)benzothiazolato-N,C$^{2'}$]iridium (acetylacetonate) [(tbt)$_2$Ir(acac)], bis(2, 4-di-fluorophenylpyridinato)-tetrakis(1-pyrazolyl)borate iridium(III) [FIr6]) doped OIDs is studied in detail. By changing the doping concentration, we report high efficiency and luminance OIDs with decent detectivity. The (tbt)$_2$Ir(acac)-doped OID with a dopant concentration of 3 wt.% achieves a maximum luminance of 70786 cd/m^2, which is three times brighter than pure 2CzPN-based device (26454 cd/m^2). To analyze the effect of the phosphorescent doping concentration on the device, the mechanisms of spectral alterations, energy transfer, and UV-light absorption of the doping system are also discussed.

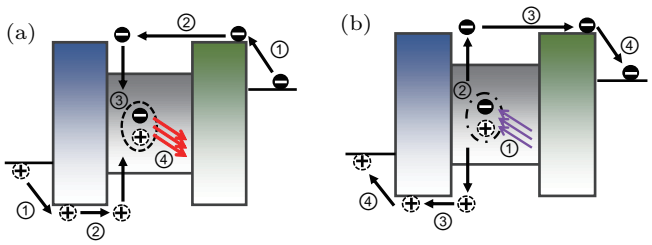


Fig. 1. (color online) (a) OIDs working in OLED mode under forward bias. (b) OIDs working in OPD mode under reverse bias.

2. Experiment details

Indium tin oxide (ITO) coated glass substrates were cleaned by detergent, deionized water, acetone, and ethanol for 15 min at each ultrasonic step. Afterwards, the substrates were dried with nitrogen gas flow and then they were treated with O_2 plasma in a vacuum chamber under a pressure of 25 Pa for 5 min to clean the surface and increase the work function of ITO. The organic functional layers and metallic cathode were thermally evaporated in a vacuum under the pressures of Pa and Pa, respectively, with a deposition rate of 0.5 Å/s. During the deposition process, the film thickness and deposition rate were monitored by an oscillating quartz crystal monitor. Phosphorescent dye doped OIDs were fabricated with a structure of ITO/MoO_3 (15 nm)/NPB (20 nm)/mCP (6 nm)/2CzPN: phosphorescent dye (10 nm, 5 wt.%)/Bphen (30 nm)/Mg: Ag (100 nm), as shown in Fig. 2(a), NPB and Bphen were used as the hole and electron transporting layers, respectively, and mCP was used as an exciton adjusting layer. Three typical phosphorescent dyes of Ir(piq)$_3$, (tbt)$_2$Ir(acac), and FIr6 were selected for device A1, device A2, and device A3, respectively, with a doping concentration of 5 wt.%, and non-doped device A4 was used as a reference. The triplet energy level of the emitting layer materials is shown in Fig. 2(b).

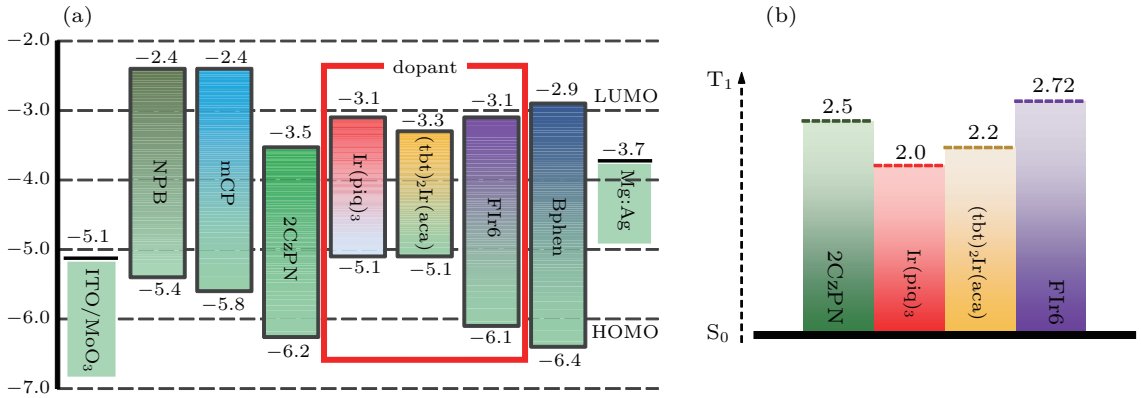


Fig. 2. (color online) (a) Schematic energy level diagram of the OIDs. (b) Triplet energy level of the emitting layer materials.

The current density–voltage–luminance (*J*–*V*–*L*) characteristics and current density–voltage (*J*–*V*) characteristics in the dark and under illumination were measured using Keithley 4200 semiconductor characterization system, and 350 nm UV light source with a power of 1.0 mW/cm^2 was used as the illumination source. The EL spectra of the devices were recorded with an OPT-2000 spectrophotometer. UV–visible (UV-vis) absorption spectra were obtained with a Shimadzu UV-1700 spectrophotometer. All the measurements were performed in air at room temperature without encapsulation.

3. Results and discussion

3.1. Influence of phosphorescent dye varieties

In order to study the influence of phosphorescent dye varieties on the OID performance, three typical emitting phosphorescent dyes are chosen as the dopant, which are red phosphorescent dye Ir(piq)$_3$, orange phosphorescent dye (tbt)$_2$Ir(acac), and blue phosphorescent dye FIr6. When the OIDs operate in the OLED mode, holes travel from the ITO/MoO_3 into the active layer, while electrons transport from the Mg: Ag cathode into the active layer, and finally the holes and electrons combine in the active layer of 2CzPN.[15] The EL spectra of these devices are displayed in Fig. 3(a). Only typical emitting peaks from (tbt)$_2$Ir(acac) (562 nm, 600 nm) are observed in device A2 without any signal of 2CzPN, this suggests that a complete Förster energy transfer is ensured without any energy back transfer.[29] In the case of device A1, the emission spectrum still contains a component of 2CzPN host (520 nm), resulting from the incomplete Förster energy transfer from the host to the guest molecules. In contrast, the EL spectrum of device A3 only exhibits the characteristic emission features of 2CzPN, this is probably due to the fact that the energy gap (E_g = |HOMO–LUMO|) of FIr6 (3 eV) is higher than that of 2CzPN (2.7 eV), so energy cannot transfer from 2CzPN to FIr6.

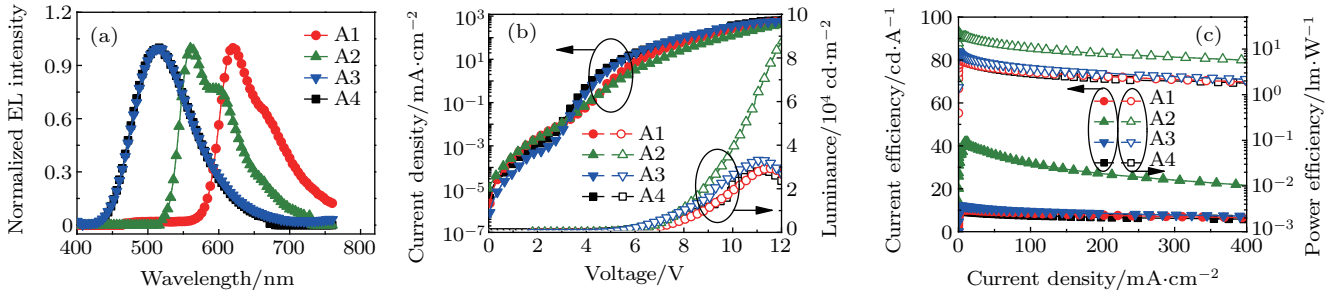


Fig. 3. (color online) (a) EL spectra of OIDs with different doping materials under 7 V forward bias. (b) Current density–voltage–luminance curves. (c) Power efficiency–current density–current efficiency curves of OIDs.

Figure 3(b) presents the *J*–*V*–*L* characteristics of the devices with and without doping phosphorescent dye, and their detailed OLED parameters are summarized in Table 1. Device A3 has a turn-on voltage of 2.7 V corresponding to 1 cd/m^2, while devices A1 and A2 have much higher turn-on voltages of 3.7 V and 3.6 V. In contrast to those of Ir(piq)$_3$ and (tbt)$_2$Ir(acac), the highest occupied molecular orbital (HOMO) and the lowest unoccupied molecular orbital (LUMO) levels of FIr6 are more adjacent to the HOMO level of mCP and the LUMO level of Bphen, which facilitates the injection and transport of holes and electrons and leads to the low turn-on voltage. The maximum brightnesses of 27083 cd/m^2, 88774 cd/m^2, 33186 cd/m^2, and 26454 cd/m^2 are achieved for devices A1, A2, A3, and A4, respectively. It is obvious that device A2 has the highest luminance among these devices.

Table 1. EL properties of OIDs doped with three different phosphorescent materials. V_{on} is the turn-on voltage, and L_{max}, PE_{max}, and LE_{max} are the maximum luminance, power efficiency, and current efficiency, respectively.

Devices	V_{on}[a]/V	L_{max}/(cd/m^2)	CE_{max}/(cd/A)	CE[b]/(cd/A)	PE_{max}/(lm/W)	PE[b]/(lm/W)
A1	3.3	26454	9.27	9.19	6.91	6.58
A2	3.7	27083	9.31	9.06	5.50	5.10
A3	3.6	88774	42.18	41.01	25.16	22.39
A4	2.7	33186	10.57	11.82	8.18	8.40

[a]Recorded at 1 cd/m^2. [b]Recorded at 100 cd/m^2.

Figure 3(c) shows the power efficiency–current density–current efficiency (PE–*J*–CE) characteristics of these devices, and their detailed OLED parameters are summarized in Table 1. The maximum CEs are 9.31 cd/A for device A1, 42.18 cd/A for device A2, 10.57 cd/A for device A3, and 9.27 cd/A for device A4, while the maximum PEs of the devices follow the same trend as that of the CEs. Device A2 shows the highest efficiency, this probably can be attributed to the efficient energy transfer from 2CzPN to (tbt)$_2$Ir(acac). As shown in Fig. 2(a), the LUMO level of Ir(piq)$_3$ is higher

than that of $(tbt)_2Ir(acac)$, leading to more trapping electrons, which then decrease the performance of device A1. For device A3, energy cannot transfer from 2CzPN to FIr6, so the characteristic of the phosphorescent dye does not show.

When a reverse bias is applied, the device functions as a UV-PD. Excitons are generated initially in the 2CzPN layer under 350 nm UV light illumination with an incident power of 1 mW/cm^2. When transporting to nearby mCP/2CzPN interface, the excitons are dissociated into holes and electrons, which are collected by the electrodes under the reverse voltage bias.[14] The current density–voltage (J–V) characteristics of the four devices in the dark and under 1 mA/cm^2 UV light are depicted in Fig. 4(a). At -2 V, the dark current densities (J_{dark}) are 9.39×10^{-7} mA/cm^2, 6.09×10^{-7} mA/cm^2, 1.10×10^{-6} mA/cm^2, and 2.17×10^{-9} mA/cm^2 for devices A1, A2, A3, and A4, respectively. When doping phosphorescent dye into 2CzPN, the light current density J_{light} also decreases. For all devices, the photocurrent density J_{light} is drastically enhanced with increasing reverse bias under the illumination of 350 nm UV light.

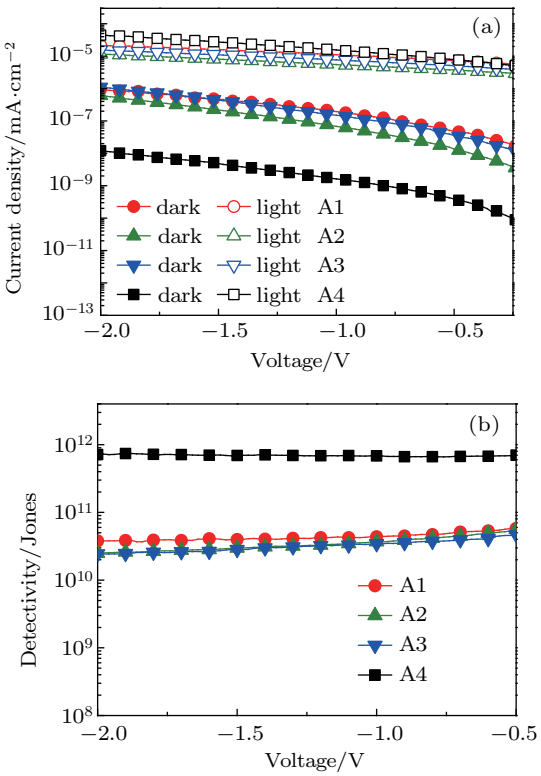


Fig. 4. (color online) (a) Light and dark current density characteristics of the OIDs measured under UV-350 nm light and in dark. (b) UV detectivity as a function of the reverse bias.

Detectivity D^* is introduced as the figure-of-merit for exhibiting the performance of UV-OPDs, which is widely employed to characterize the sensitivity of a photodetector and can be calculated as follows:

$$D^* = R/(2qJ_{dark})^{1/2} = \left(J_{light} - J_{dark}/P\right)/(2qJ_{dark})^{1/2}, \quad (1)$$

where R is the responsivity, q is the electron charge, and P is the power efficiency of the ultraviolet source.[30] Figure 4(b) presents the detectivity characteristics at different applied voltages for the four OIDs. It is obvious that device A4 has the best detectivity of 7.15×10^{11} Jones, while devices A1, A2, and A3 have similar detectivity of 3.79×10^{10} Jones, 2.52×10^{10} Jones, and 2.43×10^{10} Jones, respectively. As expected, doping phosphorescent dye into 2CzPN will reduce the detectivity, and the performance of devices doped different phosphorescent dyes is similar. It should be pointed out that 2CzPN has the charge transfer feature because of spatially separated donor and acceptor moieties. Thus, charge transfer excitons generated in the 2CzPN layer can be directly dissociated into holes and electrons and finally collected by the corresponding electrodes under a reverse bias. When doping a phosphorescent dye into 2CzPN, the heavy metal ions of the phosphorescent dye may trap the dissociated carriers, then decrease the performance of the OPD.

3.2. Influence of phosphorescent doping concentration

As the $(tbt)_2Ir(acac)$ doped device shows the highest OLED performances among the three phosphorescent dyes, four different doping concentrations of 1 wt.%, 3 wt.%, 5 wt.%, and 7 wt.% are chosen to analyze the influence of the $(tbt)_2Ir(acac)$ doping concentration on the OLED and UV-OPD performance. The notations of devices B1 (1 wt.%), B2 (3 wt.%), B3 (5 wt.%), and B4 (7 wt.%) are used to denote the corresponding devices. Figure 5(a) exhibits the UV-vis absorption and PL spectra of the neat films. The singlet and triplet metal to ligand charge transfer (^{1}MLCT and ^{3}MLCT) bands for $(tbt)_2Ir(acac)$ fall at 450 nm and 485 nm, respectively, while the other absorption features at higher energies (300–350 nm) are assigned mostly to $^3(\pi \rightarrow \pi^*)$ transitions of ligand-centered states (LC).[31] There is a spectral overlap between the PL spectrum of 2CzPN and the ^{1}MLCT absorption band of $(tbt)_2Ir(acac)$, indicating efficient FRET from 2CzPN to $(tbt)_2Ir(acac)$. The normalized EL spectra of these devices are shown in Fig. 5(b). All the EL spectra show typical $(tbt)_2Ir(acac)$ emission with a peak of 564 nm and a shoulder of 602 nm, while device B1 also contains a component of 2CzPN host as the doping concentration is too low to harvest triplet excitons in the emitting layer without any energy back transfer. Besides, the almost overlapped EL spectra of device B2 at different voltages (inset in Fig. 4(b)) indicate that the device configuration with well-designed energy level alignment prevents leakage current.

The J–V–L characteristics of the devices with stepped dopant concentrations of 1–7 wt.% are shown in Fig. 5(c). It is obvious that the current density is almost independent of the $(tbt)_2Ir(acac)$ concentration from 1 wt.% to 7 wt.%. As we know, there are two major EL mechanisms in doped

OLED, i.e., direct exciton formation on the dopant and host-guest energy transfer. As for the direct exciton formation, the dopant will trap charge carriers and change the charge density, resulting in a dependence of the *J*–*V* characteristics on the doping concentration. In case of host–guest energy transfer, the current density is insensitive to the guest doping concentration.[26] Therefore, the independence of the *J*–*V* curves on the dye doping concentration reveals that host–guest energy transfer dominates the EL process. From the *L*–*V* curves, it is discernible that the turn-on voltage decreases with increasing dopant concentration, which are 3.9 V and 3.45 V for devices B1 and B4, respectively. Device B3 yields the highest maximum luminance of 88744 cd/m^2 among the four devices, while devices B1, B2, and B4 show lower maximum luminance of 63113 cd/m^2, 70786 cd/m^2, and 77804 cd/m^2, respectively. It is obvious that all the devices doped with $(tbt)_2Ir(acac)$ achieve much higher maximum luminance than the pure 2CzPN-based device.

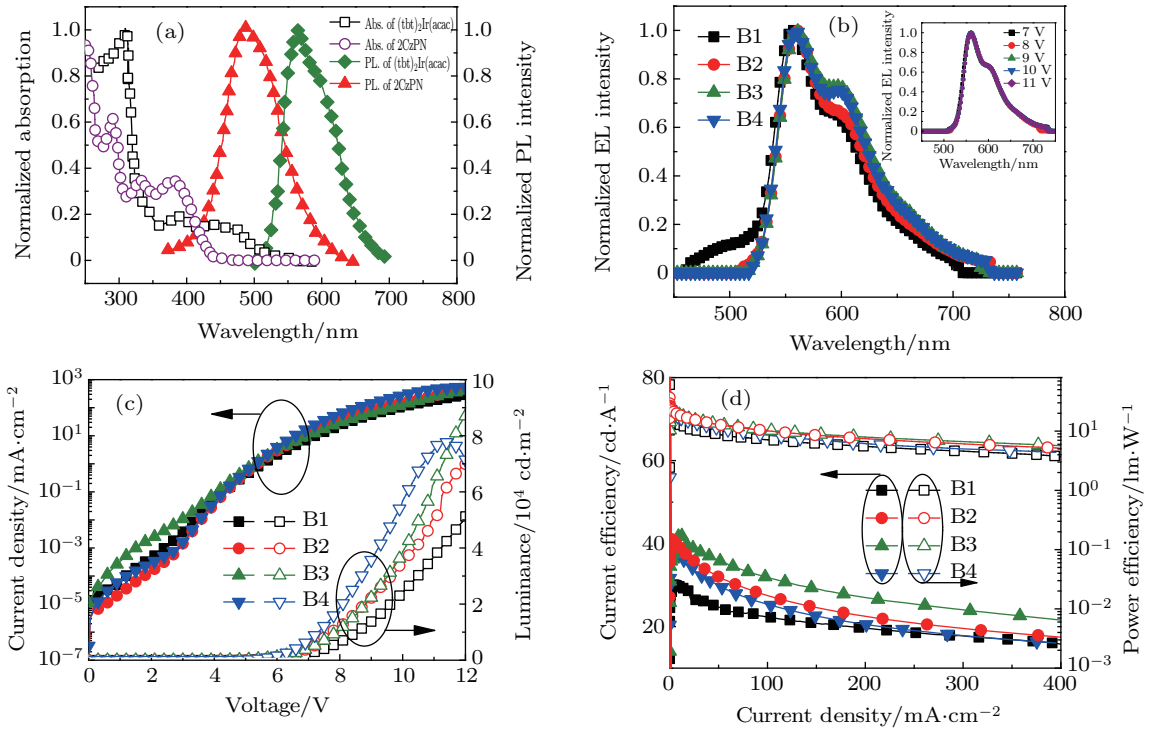


Fig. 5. (color online) (a) PL spectra and normalized UV–vis absorption spectra of $(tbt)_2Ir(acac)$ and 2CzPN neat films. (b) Normalized EL spectra of OIDs with stepped dopant concentrations. Inset: normalized EL spectra of device B2 at a driving voltage ranged from 7 V to 11 V. (c) Current density–voltage–luminance curves. (d) Power efficiency–current density–current efficiency curves of OIDs with stepped dopant concentrations.

Figure 5(d) displays the concentration-dependent PE–*J*–CE characteristics of the OIDs, while detailed OLED performance parameters are summarized in Table 2. The maximum CEs are 30.08 cd/A for device B1, 39.55 cd/A for device B2, 42.18 cd/A for device B3, and 41.10 cd/A for device B4. The highest power efficiency is obtained from the device with 5% doping concentration in the host 2CzPN, lower than the doping concentration of 7 wt% giving the highest efficiency in most phosphorescent OLEDs.[33] As we know, the triplet excitons of the traditional conventional host materials [including N,N'-dicarbazolyl-4-4'-biphenyl (CBP), 3,5'-N,N'-dicarbazole-benzene (mCP), and p-bis(triphenylsilyl)-benzene (UGH2)] are utilized by host–guest energy transfer via short-radius Dexter type. To realize efficient Dexter energy transfer, the dopant concentrations should be much higher than those of the TADF material, resulting in high cost due to the high price of rare metals in phosphors.

Table 2. EL properties of OIDs with stepped dopant concentrations.

Devices	V_{on}[a]/V	L_{max}/(cd/m^2)	CE_{max}/(cd/A)	CE[b]/(cd/A)	PE_{max}/(lm/W)	PE[b]/(lm/W)
B1	3.9	63113	30.08	29.93	16.49	14.80
B2	3.8	70786	39.55	39.41	23.92	20.97
B3	3.6	88774	42.18	41.01	25.16	22.39
B4	3.5	77804	41.10	36.78	23.25	19.40

[a]Recorded at 1 cd/m^2. [b]Recorded at 100 cd/m^2.

According to the independence of the *J*–*V* characteristics on the $(tbt)_2Ir(acac)$ doping concentration, it is obvious that host–guest energy transfer dominates the EL process. Therefore, the creation and evolution of excited states in orange device B2 can be described by Fig. 6, and the dynamical process of the excited states in the devices can be explained as follows. Singlet and triplet excitons mainly form on 2CzPN host (i), and the triplet excitons convert to singlet ones via reverse inter-system crossing (ii). Then, the singlet excitons on 2CzPN transfer to $(tbt)_2Ir(acac)$ dopant via FRET process (iii). Finally, the singlet excitons on $(tbt)_2Ir(acac)$ undergo intersystem crossing (ISC) (iv) and radiative decay for phosphorescence (v).[34] It should be noted that the efficient utilization of triplet excitons in 2CzPN for phosphorescence is responsible for the superior performance. Moreover, all excitons of the host and dopant materials can contribute to light emission, leading to the theoretical internal quantum efficiency of 100%.

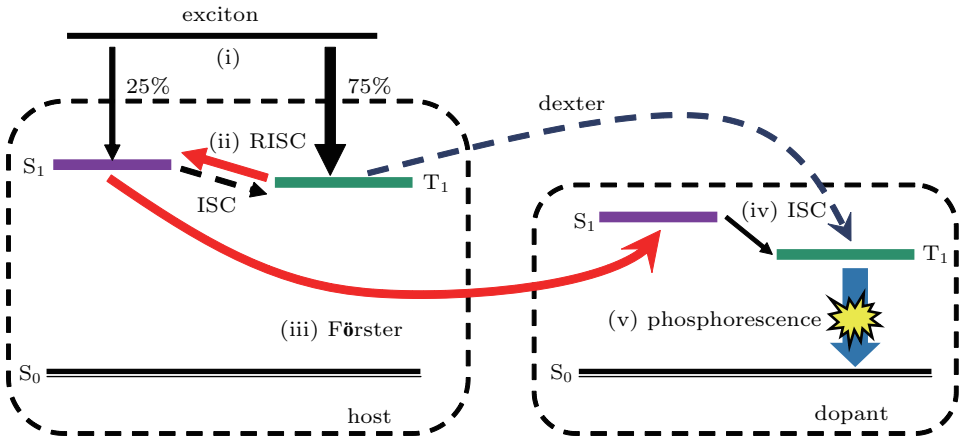


Fig. 6. (color online) Schematic diagram of emission process in the 2CzPN:$(tbt)_2Ir(acac)$-based OIDs.

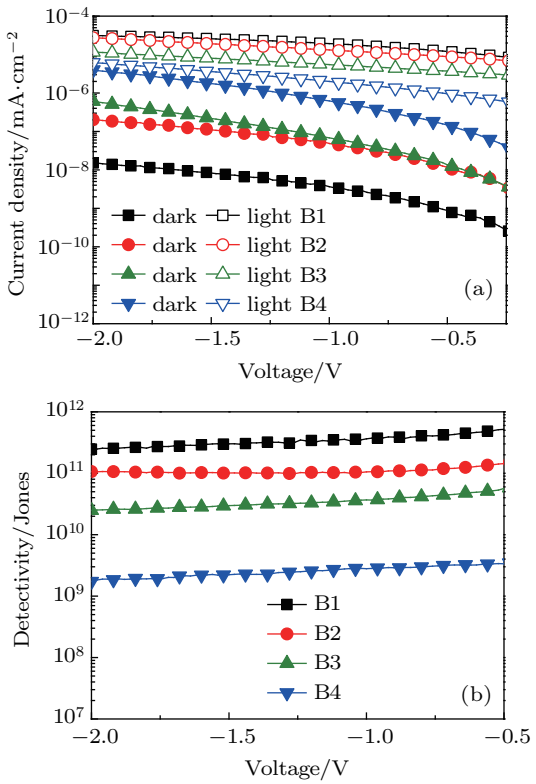


Fig. 7. (color online) (a) Light and dark current density as a function of the applied voltage of OIDs with four different concentrations. (b) UV detectivity as a function of the reverse bias.

In a reverse bias, 2CzPN is an intramolecular charge transfer complex so as to dissociate photo-induced excitons directly. Moreover, as Fig. 5(a) shows, the high absorption coefficient of 2CzPN ensures the productivity of photo-generated charges under UV light illumination.[32] The *J*–*V* characteristics of the OIDs operating in UV-OPD mode are displayed in Figs. 7(a) and 7(b), indicating the concentration dependence of the UV detective performance. The detectivity at −2 V of devices B1, B2, B3, and B4 is 4.47×10^{11} Jones, 1.07×10^{11} Jones, 2.49×10^{10} Jones, and 1.73×10^{9} Jones, respectively. With the concentration increasing, the dark current density also increases. It is obvious that when the doping concentration is higher than 3 wt.%, the doped phosphorescent dye will influence the transfer of the carriers, resulting in nearly no OPD characteristics for the OIDs. However, when the doping concentration is 3 wt.%, the OIDs could have both high EL property and decent detectivity.

4. Conclusion

The EL properties and UV detectivity of 2CzPN-based OIDs are systematically investigated via material varieties and concentration analysis of doped phosphorescent. $Ir(piq)_3$, $(tbt)_2Ir(acac)$, and FIr6, which hold different energy levels and emitting color, are chosen as the doped materials. It is proved that a deeper HOMO of phosphorescent contributes to a lower turn-on voltage under OLED mode, and through doping $(tbt)_2Ir(acac)$ into the TADF host, the OLED mode achieves the maximum current efficiency, power efficiency, and luminance of 42.18 cd/A, 25.16 lm/W, and 88774 cd/m^2, respectively, significantly improving the performance of OLED. In

contrast, all devices doped with phosphorescent have similar lower detectivity than the pure 2CzPN-based device. Moreover, the device with 3 wt.% doped $(tbt)_2Ir(acac)$ shows the maximum current efficiency, power efficiency, and luminance of 39.55 cd/A, 23.92 lm/W, and 70786 cd/m^2, respectively. Under a reverse bias, the device achieves a detectivity of 1.07×10^{11} Jones. It is obvious that the device not only shows high luminance and efficiency, but also has decent OPD performance. According to the schematic diagram of the emission process, the efficient utilization of triplet excitons in 2CzPN for phosphorescence is responsible for the superior performance. The results suggest the high potential of phosphorescent materials as guests to realize OIDs with high efficiency.

References

[1] Seino Y, Sasabe H, Pu Y J and Kido J 2014 *Adv. Mater.* **26** 1612

[2] Ou Q D, Zhou L, Li Y Q, Shen S, Chen J D, Li C, Wang Q K, Lee S T and Tang J X 2014 *Adv. Funct. Mater.* **24** 7249

[3] Zhou N, Lin H, Lou S J, Yu X, Guo P, Manley E F, Loser S, Hartnett P, Huang H, Wasielewski M R, Chen L X, Chang R P H, Facchetti A and Marks T J 2014 *Adv. Energy Mater.* **4** 1300785

[4] Peng F, Zhao B F, Xu J, Zhang Y H, Fang Y W, He R F, Wu H B, Yang W and Cao Y 2016 *Org. Electron.* **29** 151

[5] Choi E Y, Eom S H, Song C E, Nam S Y, Lee J, Woo H Y, Jung I H, Yoon S C and Lee C J 2017 *Org. Electron.* **46** 173

[6] Tang C W and VanSlyke S A 1987 *Appl. Phys. Lett.* **51** 913

[7] Zhang Q S, Li B, Huang S P, Nomura H, Tanaka H and Adachi C 2014 *Nat. Photon.* **8** 326

[8] Reineke S, Lindner F, Schwartz G, Seidler N, Walzer K, Lussem B and Leo K 2009 *Nature.* **459** 234

[9] Gong X, Tong M H, Xia Y J, Cai W Z, Moon J S, Cao Y, Yu G, Shieh C L, Nilsson B and Heeger A J 2009 *Science* **325** 1665

[10] Guo B, Wu G, Chen H Z and Wang M 2016 *Org. Electron.* **29** 13

[11] Huang J, Wang H Y, Qi Y G and Yu J S 2014 *Appl. Phys. Lett.* **104** 203301

[12] Aydemir M, Haykır G, Battal A, Jankus V, Sugunan S K, Dias F B, Al-Attar H, Türksoy F, Tavaslı M and Monkman A P 2016 *Org. Electron.* **30** 149

[13] Lu J S, Zheng Y, Chen Z J, Xiao L X and Gong Q H 2007 *Appl. Phys. Lett.* **91** 201107

[14] Wang H Y, Zhou J, Wang X, Lu Z Y and Yu J S 2014 *Appl. Phys. Lett.* **105** 063303

[15] Wang X, Zhou D L, Huang J and Yu J S 2015 *Appl. Phys. Lett.* **107** 043303

[16] Ali F, Periasamy N, Patankar M P and Narasimhan K L 2011 *J. Phys. Chem. C* **115** 2462

[17] Zhou D L, Zheng X J, Wang H Y, Huang J, Luo Y J, Zhou J, Yu J S and Lu Z Y 2016 *Synth. Met.* **220** 323

[18] Wang Z J, Zhao J, Zhou C, Qi Y G and Yu J S 2017 *Chin. Phys. B* **26** 047302

[19] Tao Y, Yuan K, Chen T, Xu P, Li H H, Chen R F, Zheng C, Zhang L and Huang W 2014 *Adv. Mater.* **26** 7931

[20] Liu W, Zheng C J, Wang K, Zhang M, Chen D Y, Tao S L, Li F, Dong Y P, Lee C S, Ou X M and Zhang X H 2016 *ACS Appl. Mater. Inter.* **8** 32984

[21] Chen J X, Liu W, Zheng C J, Wang K, Liang K, Shi Y Z, Ou X M and Zhang X H 2017 *ACS Appl. Mater. Inter.* **9** 8848

[22] Zhou D L, Wang R, Guo H, Huang J and Yu J S 2017 *Org. Electron.* **41** 355

[23] Baldo M A, O'Brien D F, You Y, Shoustikov A, Sibley S, Thompson M E and Forrest S R 1998 *Nature* **395** 151

[24] Adachi C, Baldo M A, Thompson M E and Forrest S R 2001 *J. Appl. Phys.* **90** 5048

[25] Sasabe H, Takamatsu J, Motoyama T, Watanabe S, Wagenblast G, Langer N, Molt O, Fuchs E, Lennartz C and Kido J 2010 *Adv. Mater.* **22** 5003

[26] Wang X, Zhou J, Zhao J, Lu Z Y and Yu J S 2015 *Org. Electron.* **21** 78

[27] Zhang D D, Duan L, Li Y L, Zhang D Q and Qiu Y 2014 *J. Mater. Chem. C* **2** 8191

[28] Zhang D D, Duan L, Zhang D Q, Qiao J, Dong G F, Wang L D and Qiu Y 2013 *Org. Electron.* **14** 260

[29] Qi Y G, Zhao J, Wang X, Yu J S and Chi Z G 2016 *Org. Electron.* **36** 185

[30] Lao Y F, Perera A G U, Li L H, Khanna S P, Linfield E H and Liu H C 2014 *Nat. Photon.* **8** 412

[31] Wei X Q, Peng J B, Cheng J B, Xie M G, Lu Z Y, Li C and Cao Y 2007 *Adv. Funct. Mater.* **17** 3319

[32] Fang Y J, Guo F W, Xiao Z G and Huang J S 2014 *Adv. Opt. Mater.* **2** 348

[33] Tsai M H, Lin H W, Su H C, Ke T H, Wu C C, Fang F C, Liao Y L, Wong K T and Wu C I 2006 *Adv. Mater.* **18** 1216

[34] Liu Z, Lei Y, Fan C J, Peng X F, Ji X X, Jabbour G E and Yang X H 2017 *Org. Electron.* **41** 237